Computational characterization of the vortex generated by a Vortex Generator on a flat plate for different vane angles

A. Urkiola [a], U. Fernandez-Gamiz [a,*], I. Errasti [a], E. Zulueta [b]

[a] *Nuclear Engineering and Fluid Mechanics Department, University of the Basque Country, Nieves Cano 12, 01006 Vitoria-Gasteiz, Araba, Spain*
[b] *Automatic and Simulation Department, University of the Basque Country, Nieves Cano 12, 01006 Vitoria-Gasteiz, Araba, Spain*

a b s t r a c t

Vortex generators (VGs) are usually employed to improve the aerodynamic performance for both spatial or energy issues; such as aircrafts and wind turbine blades. These structures present poor aerodynamic performance in the sections close to the hub enabling the lift to decay under critical conditions. One way to overcome this drawback is the use of VGs, avoiding or delaying the boundary layer separation. The main goal of this work is to characterize the size of the primary vortex generated by a single VG on a flat plate by Computational Fluid Dynamics simulations using OpenFOAM code. This is performed by assessing the half-life radius of the vortex and comparing it with experimental results. In addition, a prediction model based on two elementary parameters has been developed to describe in a simple way the evolution of the size of the primary vortex downstream of the vane for four different incident angles.

1. Introduction

Flow separation control has become a very important task due to its importance in many industrial applications related to Fluid Mechanics in the last decades of the past century. The most rel- evant reason of flow separation is the lack of momentum in the boundary layer which makes lift decrease and consequently turns the system into an unstable one. For instance, Taylor [21–23] and Wentz [28] investigated vortex generators (VGs) applied in aerody- namics in order to avoid this non-attached condition. An optimal design of these flow control passive devices, known as VG, could transfer high momentum from the outer side to the inner part of the layer, as sketched in Fig. 1, remaining the flow attached to the wall and ensuring stable conditions, according to Rao and Kariya
[16] and Gibertini et al. [10].

VGs are widely used both on airplane wings and wind turbine blades because they enable the use of slender blades allowing less weight for the same load distribution. These flow control devices can be mounted on blades that do not perform as expected. VGs are commonly dimensioned in relation to the local boundary layer thickness δ in order to obtain an optimal interaction between the generated vortex and the local boundary layer (BL). Depending on the flow control application, the height h of these devices could be smaller than the boundary layer as demonstrated by Ashill, Fulker

and Hackett [3] and Lin [13]. VGs are frequently triangular or rect- angular vanes positioned at an incident angle with respect to the oncoming flow and placed in groups of two or more upstream the flow Anderson [1].

Bearing in mind how important VGs are to prevent or delay the flow separation, basic research has previously occupied several re- searchers: Fernandez-Gamiz et al. [7] studied the influence of some parameters of these particular devices such as the incident angle dependency, Ünal and Gören [24] the effect on a flow around a circular cylinder, Velte [27] and Fernandez-Gamiz et al. [9] self- similarity and helical symmetry, Fernandez-Gamiz, Zamorano and Zulueta [8] vortex path variation with the height and so on. All this research is based on different theoretical models as the one proposed by Smith [19] or Velte, Hansen and Okulov [26] whose main objective was to demonstrate the helical symmetry of the vortices generated by a passive rectangular vane-type vortex gen- erator. Reader should notice that most of the models are based on the experimental BAY-model proposed by Bender [5] where body forces were used as source terms in the Navier–Stokes equations to simulate the presence of a vane.

The main purpose of this study is to characterize the size of the generated vortex by employing computational simulation. Compu- tational Fluid Dynamics (CFD) simulation has been performed con- sidering four different incident angles and validated not only ana- lytically but also experimentally. The CFD simulations presented in this work have been carried out using the OpenFOAM [15] open source code. This non-commercial code can be optimized and cus- tomized to satisfy any kind of physical phenomenon according to

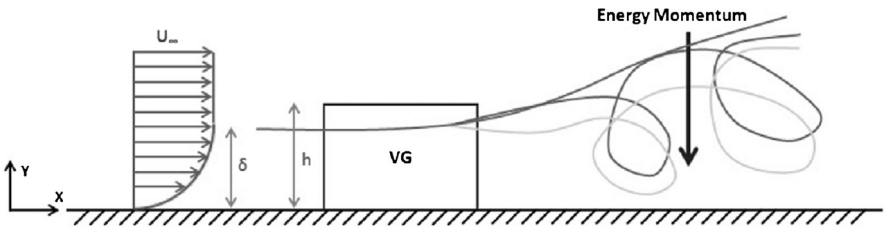

Fig. 1. Boundary layer alteration by a rectangular vortex generator on a flat plate.

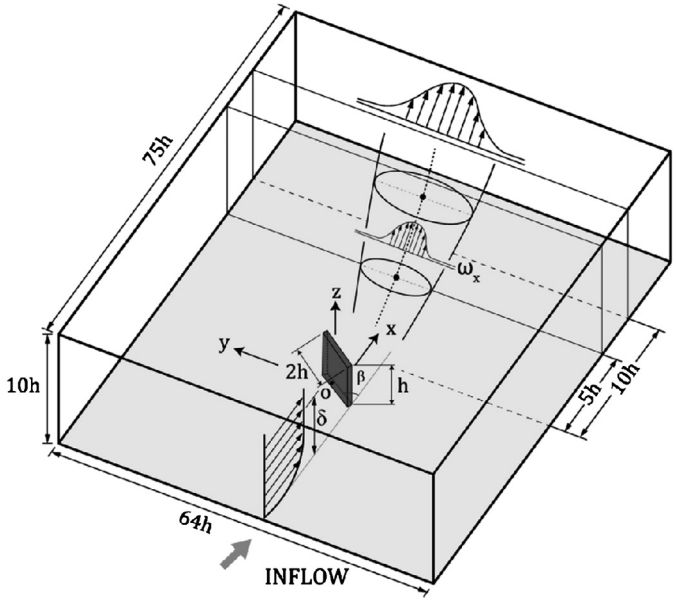

Fig. 2. Sketch of the computational domain where a rectangular vortex generator of height h is located on a flat plate at a specific incident angle of attack β with respect to the oncoming flow.

VG height h. The computational domain's width and height are 64 times and 10 times the vortex generator height h respectively. The third dimension corresponds to the length which is 75 times the vortex generator height to capture the vortex generated.

There are several features that should be taken into account when focusing on the Fig. 2. Firstly, the computational domain is dimensioned according to previous published studies by Fernandez-Gamiz et al. [9] and Fernandez-Gamiz, Zamorano and Zulueta [8] where a similar computational setup was used Secondly, some details of the wake downstream of the vortex generator can be distinguished such as the axial vorticity ω_x of the generated vortex. Fig. 2 shows how the vortex increases its size as the distance to the trailing edge of the vortex generator gets bigger. In addition, the values of the axial vorticity ω_x of the vortex are ruled by a Gaussian distribution according to Lamb [12] and Squire [20]: the maximum value of the axial vorticity is obtained at the center of the vortex and its minimum value (ω_x 0) in the regions where there is no vortex influence. Finally, the location of the particular device has been determined according to Schlichting [18] who stated that the development of the boundary layer thickness δ is related to the axial Reynolds Number Re_x:

$$\delta = \frac{0.37 \cdot x}{\sqrt[5]{Re_x}} \quad [\mathrm{m}] \qquad (1)$$

user needs. The present study compares the numerical results ob-

$$Re_x = \frac{U_\infty \cdot x}{\nu} \quad [-] \qquad (2)$$

tained by means of CFD simulations with the experimental ones achieved in wind tunnels by Bray [6]. Finally, the CFD simulations have also been validated with the analytical model of Velte [27]. In this case, the velocity profiles have been evaluated and compared. As mentioned, four incident angles of attack have been studied for the same Reynolds Number of 27000: β 10°, 15°, 18° and 20°.

where ν refers to the kinematic viscosity, x the axial position and finally, U_∞ the free stream velocity. Thus, the vortex generator was placed on a test section wall in such way that the local boundary layer thickness at that location was close to the VG height. The simulations have been carried out considering an oncoming flow speed of 20 m s^{-1} and a Reynolds Number Re 27000 based on the VG height as defined in the expression: =

2. Numerical setup

2.1. Computational configuration

Re_h

$$\frac{\rho \cdot U_\infty \cdot h}{\mu} =$$

[−] (3)

In order to obtain some of the main features of the vortex generated, CFD techniques have been employed. Nowadays, non- commercial and proprietary CFD codes are used to reproduce rel- atively well any physical problem. In this work, the open source code OpenFOAM [15] has been used for simulating the vortex. This open source CFD code is an object-oriented library written in C++ to solve computational continuum mechanics problems. One of its advantages is that the user can modify the code to create new solvers and applications as well as freely share the code developed. The current computational domain consists of a single rectangular vortex generator VG placed on a flat plate with a negligible pres- sure gradient at a specific incident angle β with respect to the oncoming flow as shown in Fig. 2.

The geometry dimensions of the rectangular vortex generator are defined with a length of two times its height h 0.25 m which corresponds to the local BL thickness δ. The dimensions for the computational domain $(64h \times 10h \times 75h)$ have been scaled to the where ρ is the density, μ the viscosity, h the vortex generator height and U the free stream velocity. The computational domain has been rotated to get the different incident angles of attack of 10°, 15°, 18° and 20°. The simpleFoam solver has been applied for steady-state, incompressible and turbulent flows using the RANS (Reynolds Average Navier–Stokes) equations. All along the calcu- lations, this solver uses the k-omega SST (Shear Stress Transport) turbulence model according to Menter [14]. Allan, Yao and Lin [2] observed that this turbulence model resulted in a better predic- tion of the streamwise peak vorticity and trajectory. The domain analyzed in this study is discretized with a structured type mesh made of flat hexahedral faces of around 11.5 million cells. Part of the refined mesh can be seen in Fig. 3(a). Full second order linear-upwind scheme for the discretization has been used for all computations.

An optimized mesh plays a major role in the CFD simulations as the tool that will help the user to discretize the domain. It is im- portant to identify the mesh regions where the results have to be

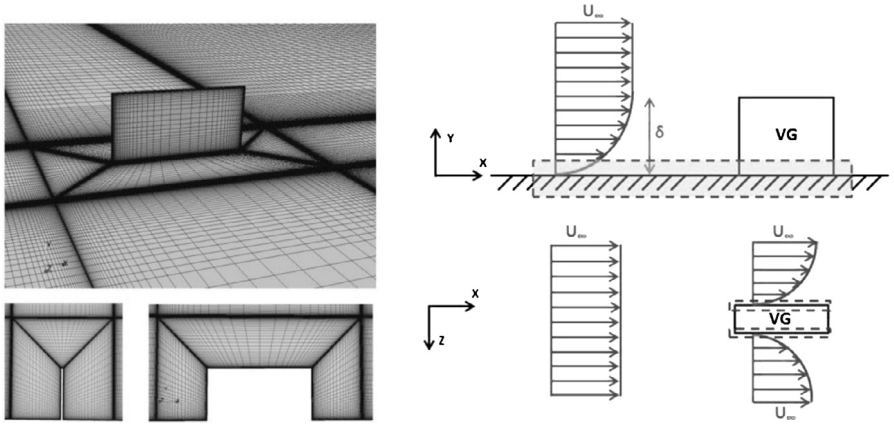

(a) Refined mesh sections around the Vortex Generator (VG). (b) Velocity profile regions under wall interaction.

Fig. 3. Mesh distribution and velocity profiles around the VG.

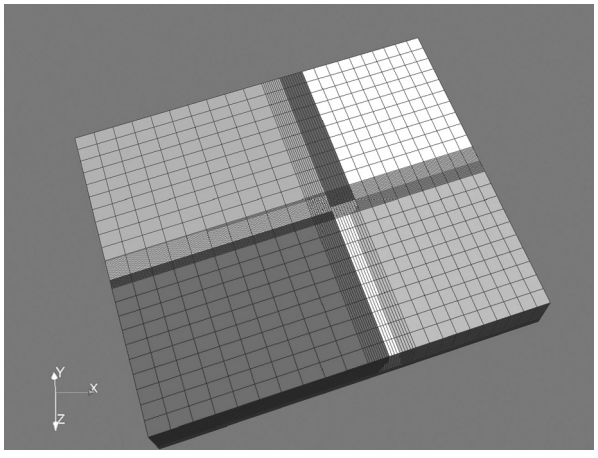

2.2. Mesh dependency study

Verification of sufficient mesh resolution was performed by a mesh dependency study based on the extrapolation proposed by Richardson and Gaunt [17]. Three different meshes have been com- pared: a finer mesh (44 blocks of 64^3 cells), a standard mesh (44 blocks of 32^3 cells) and a coarser mesh (44 blocks of 16^3 cells). The study has been carried out for two different variables such as the lift force and the drag force. In both cases the Richardson co- efficient R is less than 0.5 as shown in Table 1 which means that convergence condition is fulfilled. Any value bigger than 1 would result in divergence according to Richardson and Gaunt [17].

3. Half-life radius

Fig. 4. Decomposition of the computational domain into eight subdomains to accel- erate the solving process. The distribution of the different subdomains is indicated by a grey scale.

quite accurate as well as to establish a balance between the accu- racy of the simulations and the computational cost. Fig. 3(a) shows the block distribution around the VG and how the final mesh is refined. Fig. 3(b) illustrates the interaction between the velocity profile of the flow and the vortex generator. There are certain re- gions close to the vortex generator in which the velocity gradient changes drastically and there lies the reason why those areas are so important.

This high number of cells combined with the high amount of iterations implies a great computational cost that should be ide- ally decreased. One strategy to reduce the solving process is to decompose the domain into several subdomains and solve the sub- domains in parallel using several computer cores. In this case, the whole domain has been divided into eight subdomains as shown in Fig. 4. All the computations were carried out on a personal server-

As predicted and explained by Lamb [12] and Squire [20], the determination of the vortex radius from experimental data could result a tricky task. When analyzing the nature of the flow vortic- ity, its value would reduce to zero in the points far away from the center of the vortex according to a Gaussian distribution. Neverthe- less, this observation is not satisfied in the real case because the vorticity values do not follow the mentioned Gaussian distribution curve in points far away from the center.

Defining the radius of the vortex as the distance at which the local vorticity value is half the peak vorticity is considered to be the best method according to Bray [6]. This distance is the so- called half-life radius $R_{0.5}$ and the measurement error of the vor- ticity is negligible at this distance. As a result, there are two key parameters defining the primary vortex: the peak vorticity and the half-life radius at a streamwise position.

Fig. 5 summarizes the experimental and CFD results related to the half-life radius. The experimental results were carried out by Bray [6] by means of a parametric study of vane vortex generators. The Bray experiments were performed considering a thin rectan- gular VG with a vane aspect ratio 2:1 (height:length), free-stream velocity $U_\infty = 20\ \mathrm{m\,s^{-1}}$, incident angle of attack $\beta = 10^\circ, 15^\circ, 18^\circ, 20^\circ$, height-to-boundary layer thickness ratio $\frac{h}{\delta} = 1.639$ and Reynolds Number $Re = 27000$. This figure illustrates the compari-

2.5 GHz (8 core) and 45 GB RAM. They were converged until a satisfactory residual convergence was achieved on the velocities, pressure and turbulence fields. The computational cost took ap- proximately 90 hours. The data in the computational simulations have been obtained in different spanwise planes normal to the test section floor and positioned at a distance of five to ten times the vortex generator height h from the trailing edge of the vortex gen- erator.

son between the experimental and the CFD results for the half-life radius with similar height-to-boundary layer thickness ratio con- sidering four different incident angles of attack β: $10^\circ, 15^\circ, 18^\circ$ and 20°. All the values are normalized with respect to the vortex generator height h. The slight deviations in the results could lie on the fact that the turbulence model used to simulate the wake be- hind the VG is not able to perfectly capture the highly complex viscous interactions with the wall and the secondary structures

Table 1
Results of the mesh dependency study considering an incident angle of attack of 18° .

Variable	Mesh resolution			Richardson extrapolation		
	Coarse [N]	Medium [N]	Fine [N]	RE [N]	p	R
Drag force	98.0699	89.8929	87.199	85.875	1.6018	0.329
Lift force	261.605	247.715	241.39	236.1	1.135	0.455

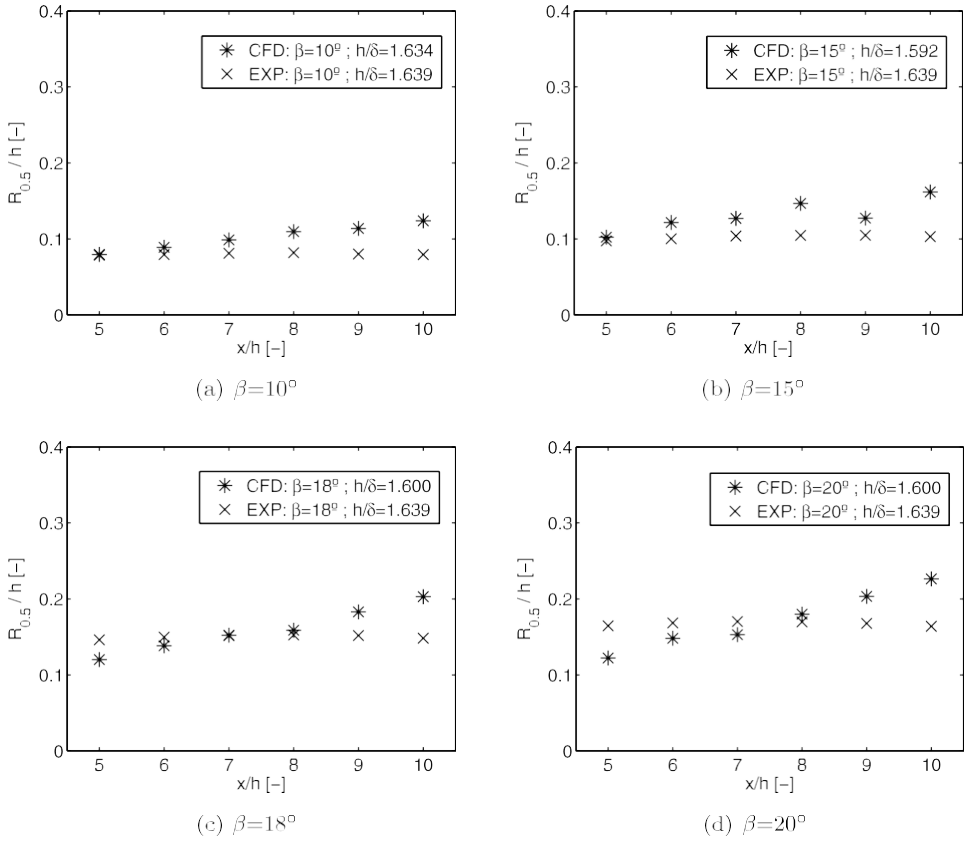

Fig. 5. Comparison between the experimental (EXP) and the CFD results of the half-life radius considering four different incident angles of attack $\boldsymbol{\beta}$: 10°, 15° , 18° and 20° . Y axis represents the normalized half-life radius $\frac{R^{0.5}}{h}$ and X axis the normalized axial distance $\frac{x}{h}$ from the trailing edge of the vortex generator.

generated by the vane. It could be concluded that the computa- tions describe relatively well the half-life radius's tendency and the value scale according to the results shown in Fig. 5.

4. Velocity profiles

This section shortly describes what has been previously cited about helical symmetry of vortices generated according to Velte, Hansen and Okulov [26] and Fernandez-Gamiz et al. [9]. When a vortex has helical symmetry, the axial u_x and azimuthal u_θ veloc- ities downstream of the VG are linearly related according to the following expression:

$$u_x = u_o - r \cdot \frac{u_\theta}{l} \quad [\mathrm{m\,s^{-1}}] \qquad (4)$$

where x is along the vortex center axis, u_0 is the vortex convec- tion velocity, r is the radial coordinate and l the helical pitch. The previous Equation (4) defining helical symmetry may be combined with those proposed by Batchelor [4] in his vortex model and the following ones are achieved:

$$[\mathrm{m\,s^{-1}}] \qquad -r^2 \qquad (5)$$

These last expressions allow the flow to be described by four parameters: the vortex core radius $\varepsilon(x)$, the circulation $r(x)$, the vortex convection velocity $u_0(x)$ and the helical pitch $l(x)$ leav- ing no restrictions on the shape of the vortex core. The analyt- ical model described in Equations (4), (5) and (6) is based on wind tunnel experiments of Velte, Hansen and Okulov [26], where SPIV (Stereoscopic Particle Image Velocimetry) measurements were taken in spanwise planes downstream of a single rectangular VG on a flat plate with a negligible streamwise pressure gradient. A turbulence-generating grid was mounted at the inlet of the wind tunnel test section with a mesh length of 39 mm. That grid was used to generate as much as necessary turbulence level to yield a high enough turbulence intensity to obtain a turbulent BL profile. The current numerical simulations were performed following the same assumptions.

An analytical validation of the velocity profiles was performed based on the computational results extracted in the cross planes positioned at distances of seven, eight, nine and ten times the vor- tex generator height h downstream from its trailing edge. Both axial and azimuthal velocity profiles have been studied at each plane position.

$$u_x(r,x) = u_0(x) - \frac{\Gamma(x)}{2\pi r}\left(1 - e^{-\frac{r^2}{\varepsilon^2(x)}}\right) \quad [\mathrm{m\,s^{-1}}] \qquad (6)$$

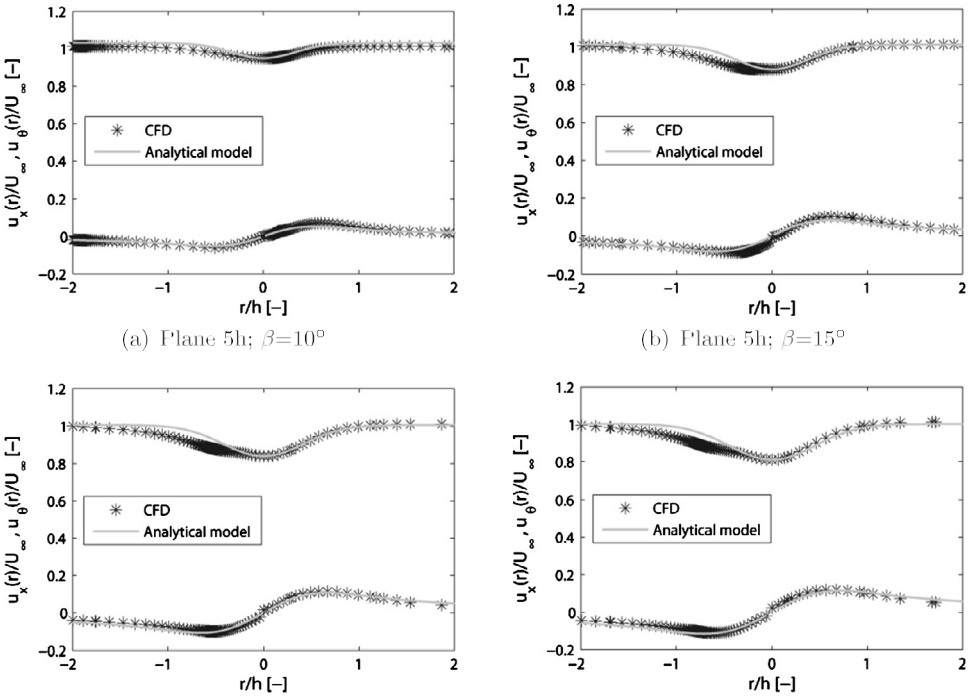

(a) Plane 5h; β=10° (b) Plane 5h; β=15°

(c) Plane 5h; β=18° (d) Plane 5h; β=20°

Fig. 6. Comparison between the analytical and CFD normalized velocity profiles at the same plane positions considering four different incident angles of attack β: 10°, 15°, 18° and 20°. Y axis represents the axial velocity (upper values) and the azimuthal velocity (lower values) and X axis the normalized radial distance $\frac{r}{h}$.

$5h$ to $10h$ downstream of the VG considering an incident angle of 18°. This angle of attack was selected for the simulations and its results compared with the analytical model because it is close to
the optimum angle found by Godard and Stanislas [11] in a para- metric study focused on the optimization of flow separation.

The two data sets corresponding to the analytical and CFD ve- locity profiles overlap reasonably well at all plane positions and different incident angles of attack. The deviation between the ana- lytical and CFD axial velocity is hardly visible. Note that there is a small deviation in the results corresponding to the negative values of the normalized radial distance r shown in Fig. 7 due to the per- turbation probably generated by a secondary vortex generation on that side in all the plots, as explained in Velte, Hansen and Okulov [26].

5. Half-life radius prediction model

After having studied individually how the normalized axial po- sition x and the incident angle of attack β influence the size of the primary vortex, the next step could be the definition of a half- life radius prediction model which would eventually include both input parameters. The analytical expression to obtain the normal- ized half-life radius based on a quadratic polynomial-type fit and function of the two mentioned parameters could be the following one:

$$\frac{R_{0.5}}{h}\left(\beta, \frac{x}{h}\right) = -74.5 \cdot 10^{-2} + 25 \cdot 10^{-3} \cdot \beta$$

between this two-dimensional fit and the CFD results are 0.9865 and 0.004957 respectively.

6. Discussion of results

It is important to understand some particularities about the evolution of the vortex center. A lateral path evolution of the vortex center exists depending on the planes beyond the trailing edge of the vortex generator and all along the simulations. Con- sequently, there is a lateral deviation of the vortex center along different axial planes. However, there is no change when focusing on the vertical path evolution; the vortex center keeps the same vertical coordinate regardless of the axial plane for distances up to fifteen times the vortex generator height h.

This nearly constant evolution of the vertical path of the vortex center was demonstrated by Fernandez-Gamiz, Zamorano and Zu- lueta [8] in a computational study of the path variation with the vortex generator height. They concluded that there was no vertical path variation for different device heights except for the lowest VG case corresponding to a 20% of the local BL thickness, for distances up to fifteen times the vortex generator height. In that case, the slope of the vertical path was much higher than the other cases. The reason could lie on the fact that due to the low height of the vane, the vortex generated is close to the inner part of the boundary layer. As a result, the viscous shear prevails and causes strong interaction with the wall. In the present study, the simu- lations are closer to the conventional example of vortex generator

$h \quad h$

$+59.4 \cdot 10^{-3}$
$+11 \cdot 10^{-3} \cdot$

x
$h +$ $-$
x
$-$

$44 \cdot 10^{-5} \cdot \beta^2$
$18 \cdot 10^{-4} \cdot$

$x \ _2 \quad [-] \qquad (7)$

height than to the smallest sub-boundary layer vortex generator case. Therefore, the results agree with the conclusion that there may be no vertical deviation of the vortex center along the ana- lyzed axial planes.

$\beta \cdot (\frac{h}{h} +$

The method employed to determine the coordinates of this vortex center is a key point in this study. Two methods have beenThis polynomial-type fit described in Equation (7) with 95% of confidence bounds and the CFD results are shown in Fig. 8. The Pearson square correlation (R^2) and root mean square error (RMSE)

used depending on which the final parameter was to be achieved. When the final target was the flow velocity profile, the point with the lowest axial velocity was considered as the center of the vor-

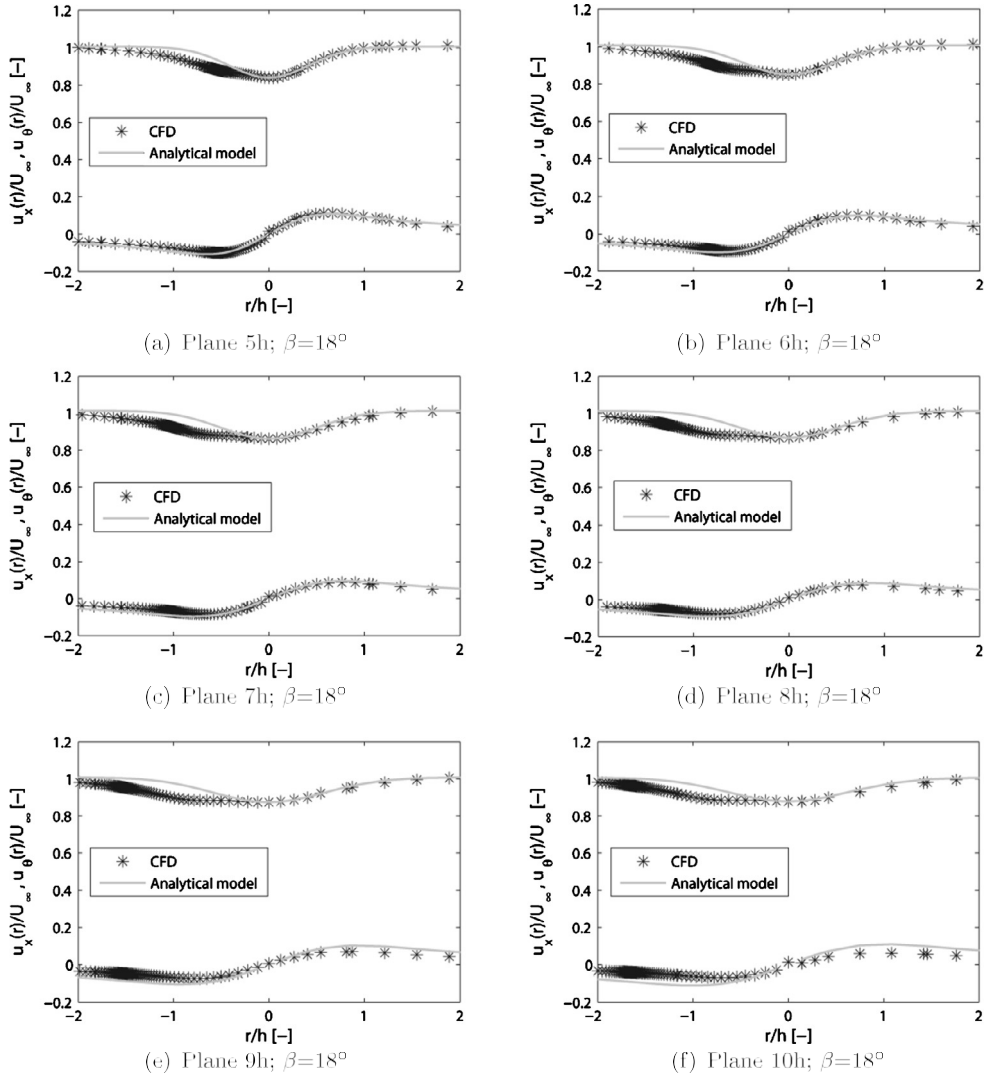

(a) Plane 5h; β=18°
(b) Plane 6h; β=18°
(c) Plane 7h; β=18°
(d) Plane 8h; β=18°
(e) Plane 9h; β=18°
(f) Plane 10h; β=18°

Fig. 7. Comparison between the analytical and CFD normalized velocity profiles at different plane positions considering an incident angle of attack of 18°. Y axis represents the axial velocity (upper values) and the azimuthal velocity (lower values). X axis represents the normalized radial distance $\frac{r}{h}$.

tex, according to the study carried out by Wygnanski, Champagne and Marasli [29]. This method was employed by Velte [27] and Fernandez-Gamiz et al. [9] when studying the mean velocity con- tours for their experiments. They concluded that there was a veloc- ity deficit in the vortex core which

became more clearly defined as the incident angle β was increased. When the final target was the vortex size, the point with the highest axial vorticity was consid- ered as the center of the vortex. This second method was checked by Yao, Lin and Allan [30] who used the peak streamwise vorticity to locate the center of the vortex core. Both methods are widely used and they provide reliable results.

Axial and azimuthal velocity profiles have been studied and compared considering two different criteria. On the one hand, the velocities profiles has been analyzed for each incident angle of at- tack individually at six streamwise plane positions as observed in Fig. 7. It can be concluded that the analytical and CFD results ac- curately match each other. However, a deviation corresponding to the negative values of the normalized radial distance r of the axial velocity profile can be appreciated which is related to the genera- tion of a secondary vortex in the CFD simulations. This asymmetry to the right side in the axial velocity profiles seems to be stronger in the CFD case. As explained by Velte [25], the influence of this secondary vortex is remarkable as the incident angle of attack in- creases. On the other hand, the second criterion consists of how the incident vane angle influences on the velocity profiles for a specific axial plane. As observed in Fig. 6, the bigger the incident angle is, the smaller is the convection velocity value and so big- ger the azimuthal velocity value is. This phenomenon makes sense because the bigger the incident angle, bigger the size of the vor- tex. The phenomenon also agrees with the results obtained by Yao, Lin and Allan [30] who used angles of attack from 10° to 23° and Fernandez-Gamiz et al. [7] starting from 20° to 35° for the quan- titative comparison.

Another point to bear in mind is how the size of the vortex has been determined by using the half-life radius $R_{0.5}$. Thus, the half-life radius is defined as the radial distance from the center of the vortex core to the point where the local vorticity is equal to half the peak vorticity according to Bray (1998). As observed in the plots shown in Fig. 5, the CFD simulations underpredict the half-life radius values at distances smaller than seven times the vortex generator height and overpredict the values for further dis- tances. In addition, the slope of the evolution of the vortex size increases as the incident angle of attack does in the computations. This means that the CFD results are much more dependent on the axial distance in comparison with the experimental results.

For small incident angles of attack such as 10° and 15° the velocity values are quite well reproduced as shown in Fig. 6. How- ever, for the incident angle of 20°, the deviation between the

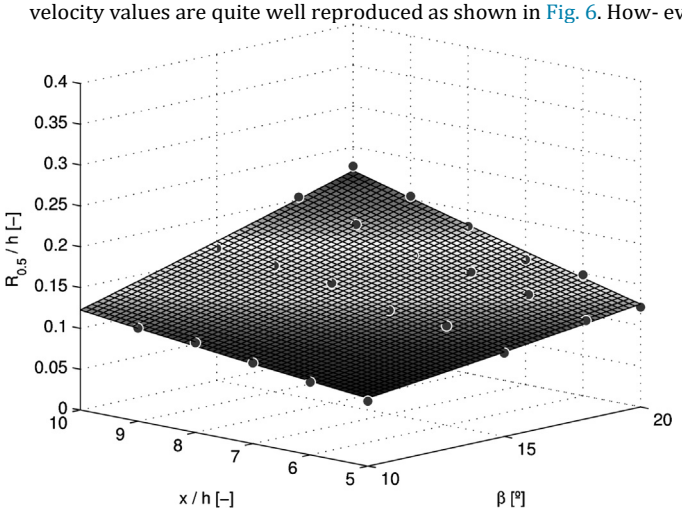

Fig. 8. CFD results of the normalized half-life radius $R_{0.5}$ as a function of the device's

The computations simulate with considerable reliability the ax- ial and azimuthal velocity profiles proposed by Velte [27]. In this case, the CFD computations have been compared with the velocity profiles calculated in this analytical model.

The present study has shown that the CFD simulations repro- duce the same kind of trends of the half-life radius of the primary vortex that those observed in the measurements of Bray [6]. Some of the main flow features of the vortex generator at the wake such as the axial and azimuthal velocity profiles are relatively well described except the highly complex viscous interactions with sec- ondary structures and the wall.

Finally, a half-life radius prediction model based on two ele- mentary parameters such as the vane incident angle of attack β and the non-dimensional downstream position x has been devel- oped. This simple model is limited to the cases investigated in the present work and consists of a quadratic polynomial-type surface which fits relatively well the computational results. This model is able to describe the vortex size evolution in a simple way andcould eventually help in the design of real VG applications (e.g.incident angle of attack β h x are indicated with

wind turbine blades or aircraft wings) where certain parametric

analytical and CFD results increases. The reason of this deviation could probably lie on the fact that the flow is partially stalled at this angle of attack. As concluded by Yao, Lin and Allan [30], the vortex radius generated by a conventional vortex generator is more dependent on the incident angle of attack in contrast to the low-profile vortex generator. In this work, it is demonstrated that vortex generators higher than the local boundary layer are doubtless dependent on the incident angle of attack. Particularly, the half-life radius $\overline{R^{0.5}}$ increases from 0.07 to 0.12 when the angles of attack change from 10° to 20° at a streamwise distance of five times the vortex generator height as depicted in Fig. 5(a) and Fig. 5(d).

Finally, the half-life radius prediction model presented in Equa- tion (7) fits relatively well the computational results for all the vane angles analyzed and the only $_h$ VG height studied, see Fig. 8. The greatest deviations between the estimated vortex half-life radius of this prediction model and the simulated half-life radius are found for the largest vane angle β 20°—at the farthest plane position ^{x} 10. The reason of these deviations could lie on the difficulty to find the vortex core center and consequently its size because the VG is probably operating near the stall conditions.

7. Conclusions

In this study, vortices generated by a passive rectangular vane- type vortex generator on a flat plate with a negligible pressure gradient are simulated. CFD simulations are carried out using the open source library OpenFOAM, considering a Reynolds Number Re 27000 and four different incident angles of attack: β 10°, 15 , 18° and 20° . The phenomenon is reproduced taking into ac- count steady-state, incompressible and turbulent flow using RANS equations which is combined with the k-omega SST turbulence model.

In order to measure the size of the primary vortex generated, its normalized half-life radius is numerically assessed by CFD tech- niques as well as experimentally validated. Values obtained of the normalized half-life radius at different axial plane positions have been compared and it could be concluded that the compu- tational model relatively well reproduces the vortex size in scale and tendency. Moreover, it is demonstrated that the vortex size is dependent on the incident angle of attack when using vortex gen- erators higher than the local boundary layer. Nevertheless, some discrepancies are visible when working with high incident angles of attack.

studies could be considerably reduced in terms of time and cost by facilitating engineering tools.

Conflict of interest statement

No conflict of interest is declared.

Acknowledgements

This work was supported by the Government of the Basque Country and the University of the Basque Country UPV/EHU through the SAIOTEK (S-PE11UN112) and EHU12/26 research pro- grams respectively.

References

[1] B.H. Anderson, The aerodynamic characteristics of vortex ingestion for the fla-18 inlet duct, NASA Lewis Research Center, Cleveland, Ohio 44135, in: 29th Aerospace Sciences Meeting, Nevada, 1991.
[2] B.G. Allan, C.S. Yao, J.C. Lin, Numerical simulations of vortex generators and jets on a flat plate, in: 1st Flow Control Conference, 24–27, AIAA, St. Louis, Missouri, 2002.
[3] P.R. Ashill, J.L. Fulker, K.C. Hackett, Research at DERA on sub boundary layer vortex generators (SBVGs), in: 39th Aerospace Sciences Meeting and Exhibit, January 8–11, 2001, AIAA, Reno, Nevada, 2001.
[4] G.K. Batchelor, Axial flow in trailing line vortices, J. Fluid Mech. 20 (1964) 645–658.
[5] E.E. Bender, B.H. Anderson, P.J. Yagle, Vortex generator modeling for Navier– Stokes codes, in: Proc. 3rd ASME/JSME Joint Fluids Engineering Conference, San Francisco, California, USA, 1999.
[6] T.P. Bray, A Parametric Study of Vane and Air-Jet Vortex Generators, PhD Thesis, Cranfield University, College of Aeronautics, 1998.
[7] U. Fernandez-Gamiz, P.E. Réthoré, N.N. Sorensen, C.M. Velte, F. Zahle, E. Egusquiza, Comparison of four different models of vortex generators, in: EWEA 2012 – European Wind Energy Conference & Exhibition, May 16–19, 2012, Denmark, Copenhagen, 2012.
[8] U. Fernandez-Gamiz, G. Zamorano, E. Zulueta, Computational study of the Vor- tex path variation with the VG height, J. Phys. Conf. Ser. 524 (2014) 012024, http://dx.doi.org/10.1088/1742-6596/524/1/012024.
[9] U. Fernandez-Gamiz, C.M. Velte, P.E. Réthoré, N.N. Sorensen, E. Egusquiza, Test- ing of self-similarity and helical symmetry in vortex generator flow simula- tions, Wind Energy (2016), http://dx.doi.org/10.1002/we.1882.
[10] G. Gibertini, J.C. Boniface, A. Zanotti, G. Droandi, F. Auteri, R. Gaveriaux, A. Le Pape, Helicopter drag reduction by vortex generators, Aerosp. Sci. Technol. (ISSN 1270-9638) 47 (2015) 324–339, http://dx.doi.org/10.1016/j.ast. 2015.10.004.
[11] G. Godard, M. Stanislas, Part 1: Optimization of passive vortex genera- tors, Aerosp. Sci. Technol. 10 (2006) 181–191, http://dx.doi.org/10.1016/j.ast. 2005.11.007.
[12] H. Lamb, Hydrodynamics, sixth edition, Dover Publications, New York, 1932.
[13] J.C. Lin, Review research on low-profile vortex generators to control boundary layer separation, Prog. Aerosp. Sci. 38 (4) (2002) 389–420, http://dx.doi.org/ 10.1016/S0376-0421(02)00010-6.F.R. Menter, Zonal two equation k–w turbulence model for aerodynamics flows, AIAA J. 932906 (1993), http://dx.doi.org/10.2514/6.1993-2906.
[14] OpenFOAM, http://www.openfoam.com, 2014.
[15] D.M. Rao, T.T. Kariya, Boundary-layer submerged vortex generators for separation control-an exploratory study, AIAA Paper 88-3546-CP in: AIAA/ASME/SIAM/APS 1st National Fluid Dynamics Congress, July 25–28, Cincinnati, OH, 1988.
[16] L.F. Richardson, J.A. Gaunt, The deferred approach to the limit. Part I. Single lattice. Part II. Interpenetrating lattices, Philos. Trans. R. Soc. Lond. Ser. A 226 (1927) 299–361, http://dx.doi.org/10.1098/rsta.1927.0008.
[17] H. Schlichting, Boundary-Layer Theory, McGraw-Hill, New York, 1968.
[18] F.T. Smith, Theoretical prediction and design for vortex generators in turbulent boundary layers, J. Fluid Mech. 270 (1994) 91–131, http://dx.doi.org/10.1017/ S0022112094004210.
[19] H. Squire, The growth of a vortex in turbulent flow (vortex growth in turbulent incompressible flow), Aeronaut. Q. 16 (1965) 302–306.
[20] H.D. Taylor, The Elimination of Diffuser Separation by Vortex Generators, Re- search Department Report No. R-4012-3, United Aircraft Corporation, East Hart- ford, Connecticut, 1947.
[21] H.D. Taylor, Application of Vortex Generator Mixing Principles to Diffusers, Research Department Concluding Report No. R-15064-5, United Aircraft Cor- poration, East Hartford, Connecticut, 1948.
[22] port No. R-05280-9, United Aircraft Corporation, East Hartford, Connecticut, 1950.
[23] U.O. Ünal, Ö. Gören, Effect of vortex generators on the flow around a circular cylinder: computational investigation with two-equation turbulence models, Eng. Appl. Comput.

Fluid Mech. 5 (1) (2011) 99–116, http://dx.doi.org/10.1080/ 19942060.2011.11015355.
[24] C.M. Velte, Simulation and Control of Wind Turbine Flows using Vortex Gener- ators, PhD Dissertation, DTU-Technical University of Denmark, Denmark, 2009.
[25] C.M. Velte, M.O. Hansen, V.L. Okulov, Helical structure of longitudinal vortices embedded in turbulent wall-bounded flow, J. Fluid Mech. 619 (2009) 167–177, http://dx.doi.org/10.1017/S0022112008004588.
[26] C.M. Velte, A vortex generator flow model based on self-similarity, AIAA J. 51 (2) (2013) 526–529, http://dx.doi.org/10.2514/1.J051865.
[27] W.H. Wentz, Effectiveness of Spoilers on the GA(W)-1 Airfoil with a High Per- formance Fowler Flap, NASA CR-2538, May 1975.
[28] I. Wygnanski, F. Champagne, B. Marasli, On the large-scale structures in two dimensional, small-deficit, turbulent wakes, J. Fluid Mech. 168 (1986) 31–71.
[29] C.S. Yao, J.C. Lin, B.G. Allan, Flow-field measurement of device-induced embed- ded streamwise vortex on a flat plate, in: 1st Flow Control Conference, 2002.